

MRI Image Segmentation of Brain Tissue by Novel Level Set Model

Chih-Yu Hsu ¹, Chih-Hung Yang ², Hui-Ching Wang ³, Hsiao-Yu Lin ⁴

1 Department of information & communication Engineering, ChaoYang University of Technology, TaichungTaiwan, R.O.C.

2 Department of Applied Mathematics, National Chung-Hsing University, Taichung, Taiwan, R.O.C.

3 Department of Applied Mathematics, National Chung-Hsing University, Taichung, Taiwan, R.O.C.

4 Department of Applied Mathematics, National Chung-Hsing University, Taichung, Taiwan, R.O.C.

¹tccnchsu@gmail.com

²48753001nchu@gmail.com

³hcwang@amath.nchu.edu.tw

⁴c5811106@hotmail.com

Abstract—In the paper, we proposed a model called Adaptive Threshold Level Set Without Edge that is applied on the segmentation of GM in brain MR images. Threshold to find the boundary of GM is automatically obtained by fuzzy c mean algorithm. A similarity index (SI) is used for quantitative evaluation of the segmentation results. By testing 134 planar MR brain images and comparing to the gold standard segmentation, the mean and the variance of SI are 0.90311 and 0.042049. The experimental results demonstrate our method can automatically and accurately segment the GM.

Keywords—Level set method, Fuzzy clustering, Gold standard, Image segmentation, MR imaging.

1. INTRODUCTION

MRI has become a particularly useful medical diagnostic tool for neurological diseases. Segmentation of magnetic resonance (MR) images is widely applied in brain function researches, radiological evaluation and 3D visualizations for surgical planning. Brain image segmentations classify the voxels into three different tissue types: grey matter (GM), white matter (WM), and cerebrospinal fluid (CSF). Segmentation methods are broadly classified into three categories: edge-based methods, pixel-based direct classification methods and region based methods [1]. Intensity based method belongs to the pixel-based direct classification

methods because the intensity is used as the features for classification. Lots of intensity-based classifiers are developed for intensity-based segmentation techniques; for example, there are neural network classifier [2][3][4][5], the k-nearest neighbor classifier [6] and standard fuzzy c-means algorithm [7][8]. Besides intensity-based segmentation techniques, active contour model [9] is a technology extracting the regions of interest (ROI) from primitive image with the contours of the ROI pixels. Geometric Active Contour model known as level set method [10][11] has recently been applied on the application of segmentation [12]. Level set methods are surface-based segmentation techniques and have the advantage for the possible reduction of the partial volume effect [13]. A image segmentation model [14] with a piecewise smooth function fitted to the image data and the discontinuities happening only on the boundaries between different tissue types is proposed to find the tissue boundaries. The boundaries of tissue are contours of this function with zero level and the solution can be obtained by either solving a partial differential equation or optimizing an objective function. Threshold Level Set Method [15][16] is a level set model. Our previous work [17] using Otsu [18] algorithm to automatically obtain two thresholds of speed functions for the threshold Level Set. However, Otsu algorithm can only find a crisp threshold, but it is not available for the fuzziness of boundary. Improving the fuzzy tissue boundary segmentation can be applied on automatically segmenting the WM of brain. A new segmentation method modified from Chan and Vese model [19] and Fuzzy C-Means

algorithm is proposed and called Adaptive Threshold Level Set Without Edge (ATLSWE) Model. By using similarity index and comparing to the gold standard image segmentations, we suggested a common fair comparison method for segmentation evaluation of brain tissues. The segmentation results of the WM by ATLSWE Model are accurate enough compared with the gold standard segmentations. We wish the other researchers use their programs and parameters to compare their results with the gold standard segmentations and our results.

2. MATERIAL AND METHOD

Accuracy evaluation is the most important issue for any new segmentation method. It is very popular for researchers to evaluate their developed method by comparing with other methods. They use their own image sources that are segmented by their method and the other methods. Comparing these results, they evaluate the accuracy of their proposed segmentation method. However, they implement the programs for the other methods and select parameters by themselves. It is possible they may not succeed the best segmentations of their implemented methods without the optimal parameters, so the evaluations may be unfair for these situations. It is necessary to find a common accuracy evaluation method that is fair for any new developed algorithm. Since the mrGray software package [20][21] provides brain MRI images and the results of WM segmentation, it is reasonable to use these segmentation results as a common gold standard for evaluating any segmentation method for brain WM in the MRI images.

MrGray software package has a T1-weighted volumetric MR image data set with DICOM format. The data set has 134 slices of MR brain images with the resolution size 204x120 pixels and the gray level ranges from 0 to 255. The resolution of the data set is fine enough to resolve the complex structure of the cortex and to provide adequate contrast between GM, WM, and CSF. The segmentation results of the WM are also provided in mrGray software package which are used as gold standard to be compared with the segmentation results by ATLSWE Model.

The flow chart of the ATLSWE Model is shown in Fig. 1. The first step is to import the brain MR image and followed by an image preprocessing, stripping the skull. The selection of threshold parameters must be performed before segmentation of the WM surface.

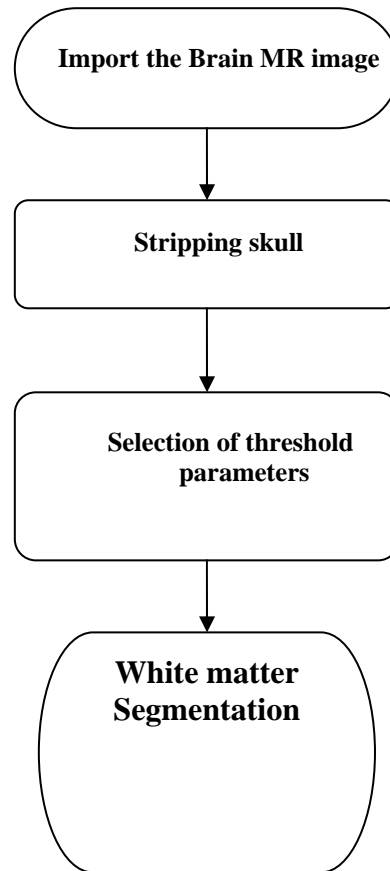


Fig. 1 Flow chart of the white matter Segmentation

To strip the skull by removing skin, bone, fat, and other non-cerebral tissues for extracting the cerebrum in the image is the second step of the follow chart. This stripping skull process can be accomplished by using mathematical morphology operators [22]. Fig. 2 (a) shows the original image of 67th slice and Fig. 2 (b) shows the image processed by stripping skull process.



(a)



(b)

Fig. 2 The 67th slice (a) original image and (b) processed result by stripping the skull.

The segmentation method of the Adaptive Threshold Level Set Without Edge (ATLSWE) Model should be described before the selection of threshold parameters because the threshold parameters is part of ATLSWE Model. The following section describes the ATLSWE Model.

2.1. Level Set Model

The ATLSWE Model is extended from the methodology of Active Contours Without

Edges that is also called Chan and Vese model [19]. The Chan and Vese model is an active contour model for segmentation of objects without explicit edges in images. We summarily described the Chan and Vese model in this section for understanding the ATLSWE Model. The Chan-Vese segmentation model evolves active contour Γ to separate a image into two regions—one region is inside Γ and the other region is outside Γ as shown in Fig. 2. The desired curve Γ_{OPT} should be located at the boundary between objects and background. The objects should be the region inside Γ , and the background to be the region outside. Intensity u_0 of an image is a function can be combined by two functions u_0^i and u_0^o . The symbols u_0^i and u_0^o denote the intensity functions for inside and outside regions of Γ . Functional $E(\vec{C})$ can be formulated as following:

$$E(\vec{C}) = \int_{inside(\Gamma)} (u_0 - c_1)^2 + \int_{outside(\Gamma)} (u_0 - c_2)^2 + \mu |\Gamma| \quad (1)$$

Where c_1 and c_2 are the averages of u_0^i and u_0^o , μ is a positive parameter and $|\Gamma|$ is the length of the evolving curves. The boundaries of objects Γ_{OPT} will be captured by the active contour Γ when the functional $E(\Gamma)$ is minimized.

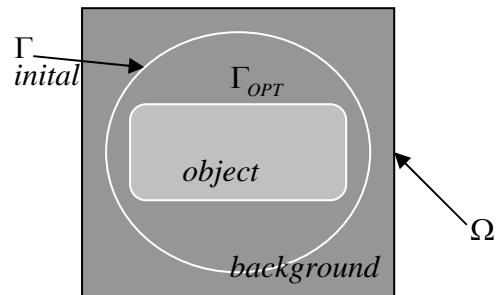


Fig. 3 Boundary Γ_{OPT} of the object and active contour Γ

The evolution curves can be represented by the zero-level lines of a surface function ϕ in R^3 . This approach $\vec{C} = \{(x, y) | \phi(x, y) = 0\}$ is called in the level set formulation, Chan and Vese introduce the level set function ϕ to the functional $E(\vec{C})$ and the equation (1) is changed as follow:

$$\begin{aligned}
 E(c_1, c_2, \phi) = & \int_{\Omega} (u_0 - c_1)^2 H(\phi) dx dy \\
 & + \int_{\Omega} (u_0 - c_2)^2 (1 - H(\phi)) dx dy \quad (2) \\
 & + \mu \int_{\Omega} |\nabla H(\phi)| dx dy
 \end{aligned}$$

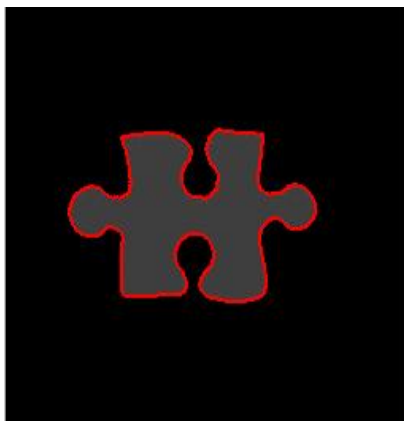
Where Ω is the total region in the image, ϕ is a level set function and H is a Heaviside function and c_1 and c_2 are average values of intensity u_0 inside and outside regions of Γ . c_1 and c_2 can be denoted as following:

$$\begin{aligned}
 c_1 = & \frac{\int_{\Omega} u_0 H(\phi) dx dy}{\int_{\Omega} H(\phi) dx dy} \\
 c_2 = & \frac{\int_{\Omega} u_0 (1 - H(\phi)) dx dy}{\int_{\Omega} (1 - H(\phi)) dx dy} \quad (3)
 \end{aligned}$$

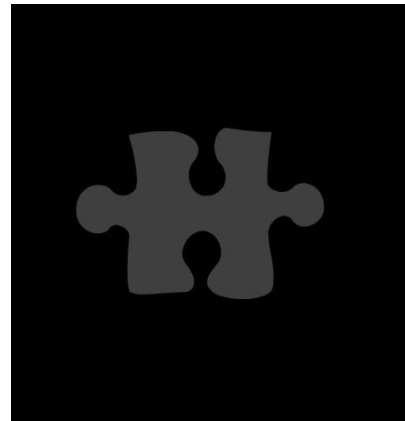
By variation calculus and conditions of c_1 and c_2 , Chan-Vese model obtained the Euler-Lagrange equation as follow.

$$\frac{\partial \phi}{\partial t} = \delta_{\epsilon}(\phi) \left(\mu \frac{\nabla \phi}{|\nabla \phi|} - |u_0 - c_1|^2 + |u_0 - c_2|^2 \right) \quad (4)$$

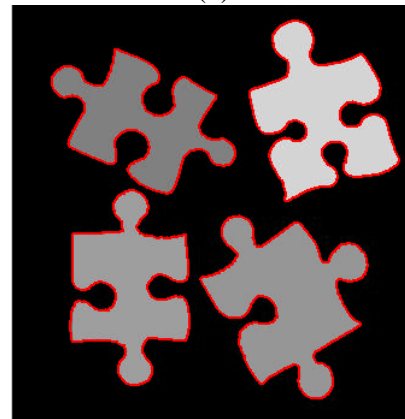
Where μ is a parameter, $\delta_{\epsilon} = H'_{\epsilon}$ is an delta function of the derivative of a approximate. Equation (4) is the Chan-Vese evolution equation used to separate object regions from background. Fig. 4 is synthetic image and the segmentation results.



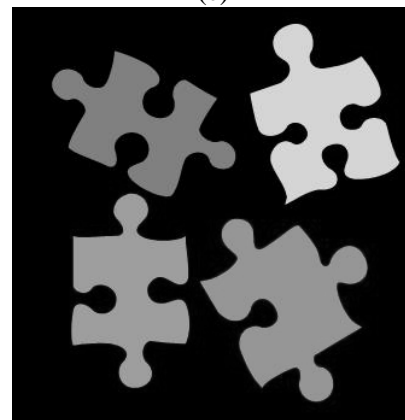
(a)



(b)



(c)



(d)

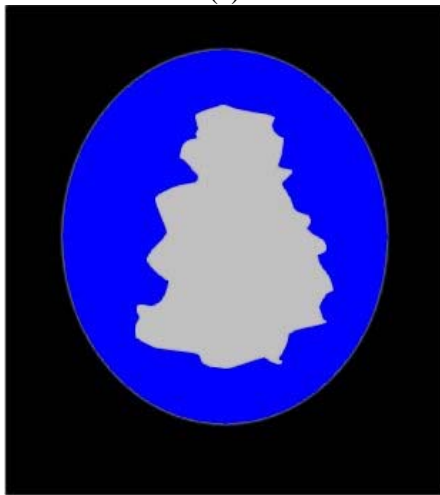
Fig. 4 Segmentation result (a)(c) and (b)(d) original image

Fig. 5 (a) is a synthetic image like a brain phantom and the blue region in Fig. 5 (b) is the desired ROI like the WM region. Fig. 5 (c) is a segmentation result obtained by Chan-Vese model and the segmentation result (the region inside the red curve) does not match our desired ROI. There are multiple regions with different grey level in an image as shown in Fig. 6(a). The region inside the red curve as shown in Fig. 6(c) is the segmentation result obtained by Chan-Vese model and does not match our desired ROI Fig.

6(b). These two examples show that Chan-Vese model is not able to effectively segment desired ROI.



(a)

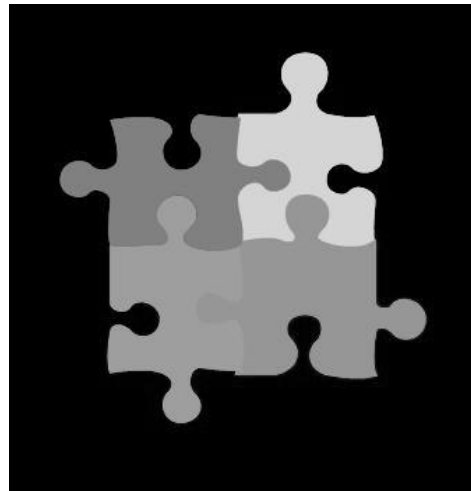


(b)

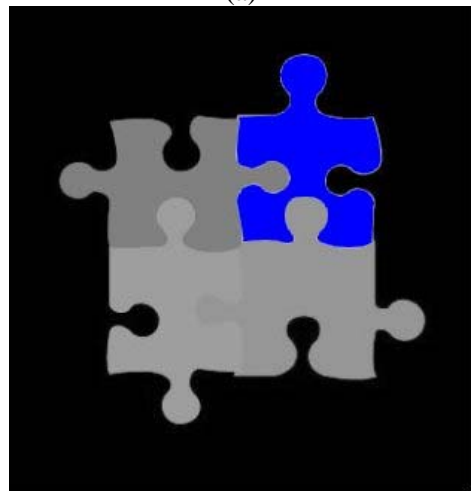


(c)

Fig. 5 The synthetic (a) original image (b) ROI (blue) and (c) segmentation result (inside red curve)



(a)



(b)



(c)

Fig. 6 The synthetic (a) original image (b) ROI (blue) and (c) segmentation result (inside red curve)

We now explain why Chan-Vese model is not able to segment the desired ROI. The location of the red active contour is decided by c_1 and c_2 that is automatically computed by the equation

(3). The computations of c_1 and c_2 are not satisfied to our desired the location of the red active contour. It is necessary adjust c_1 and c_2 to fit our desired the location to overcome the shortness.

2.2. ATLSWE Model

We proposed a solution that c_1 and c_2 are chosen to satisfy on our requirements and the idea developed the ATLSWE model. The Euler-Lagrange equation of the ATLSWE model derived in the *Appendix* can be formulated as follow :

$$\frac{\partial \phi}{\partial t} = \delta_\varepsilon(\phi)(\mu \nabla \cdot \frac{\nabla \phi}{|\nabla \phi|}) - \delta_\varepsilon(\phi)(u_0 - c_1)^2 + \delta_\varepsilon(\phi)(u_0 - c_2)^2 \quad (5)$$

Where c_1 and c_2 are constants. Equation (5) is the same as the equation 4 but they do not satisfy the same condition. Equation (4) is obtained by using the optimal conditions of c_1 and c_2 , but equation (5) is derived by setting c_1 and c_2 , constants. As shown in the *Appendix*, the same functional with different conditions obtain the same Euler-Lagrange equation. To ignore the curvature effect, we set $\mu = 0$ and equation (6) can be changed from equation (5).

$$\frac{\partial \phi}{\partial t} = \delta_\varepsilon(\phi) \left(-|u_0 - c_1|^2 + |u_0 - c_2|^2 \right) \quad (6)$$

Because of c_1 and c_2 are constants, we can simplify the equation (6).

$$\frac{\partial \phi}{\partial t} = -2\delta_\varepsilon(\phi) \left((c_2 - c_1) \left[u_0 - \left(\frac{c_1 + c_2}{2} \right) \right] \right) \quad (7)$$

In the equation (7), the constant values of c_1 and c_2 decide the location of the active contour Γ .

The value of $\frac{c_1 + c_2}{2}$ can also decide the location of the active contour Γ .

An example is shown to differentiate the segmentation capability of Chan-Vese model and the ATLSWE model. Fig. 7(a) is a synthetic image having sixteen squares with increasing gray levels from left up to right down. Segmentation result by Chan-Vese model in Fig. 7(b) shows that all sixteen squares are enclosed by the blue lines. Only six squares are enclosed by the blue lines are shown in Fig. 7(c). The

result is obtained by the ATLSWE model when the value $\frac{c_1 + c_2}{2}$ of evolution equation (7) is

155. The value $\frac{c_1 + c_2}{2}$ can be chosen to select the desired squares.

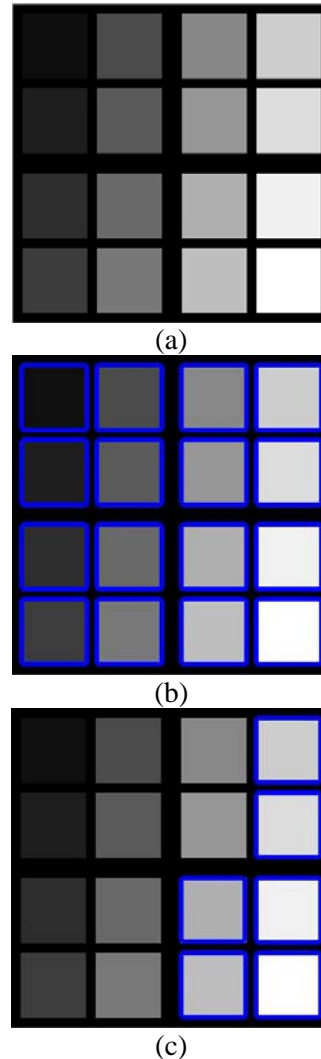


Fig. 7 (a) Synthetic image (b) segmentation result by Chan-Vese model and, and (c) segmentation

result by equation (8) with $\frac{c_1 + c_2}{2} = 155$

When an object has outer and inner contours, only one level set function to find one contour of an object is not enough. For example, GM is a band region with both outer and inner contours. We can use two level set function ϕ_1 and ϕ_2 to substitute them into the equation (7) for obtaining both outer and inner contours. Let $\phi = \phi_1$, and substitute it into the equation (7) and let

$c_3 = \frac{c_1 + c_2}{2}$. We obtain equation (8) from equation (7).

$$\frac{\partial \phi_1}{\partial t} = -2\delta_\varepsilon(\phi_1)((c_2 - c_1)(u_0 - c_3)) \quad (8)$$

Let $\phi = \phi_2$ and $c_1 = c_4, c_2 = c_5$, and substitute it into the equation (7) and let $c_6 = \frac{c_4 + c_5}{2}$. We

obtain equation (9) from equation (7).

$$\frac{\partial \phi_2}{\partial t} = -2\delta_\varepsilon(\phi_2)((c_5 - c_4)(u_0 - c_6)) \quad (9)$$

where c_5 and c_4 are constants. We use fig. 8 to explain how TLSWE model works. Fig. 8 is a synthetic image and ROI is the gray region. The gray level of ROI is between Lower Threshold and Upper Threshold.

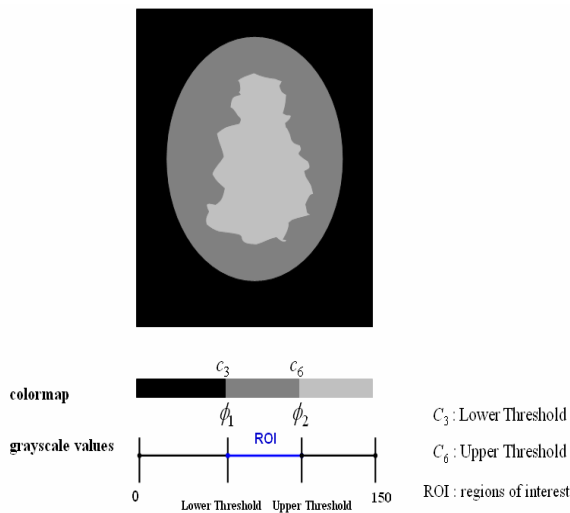
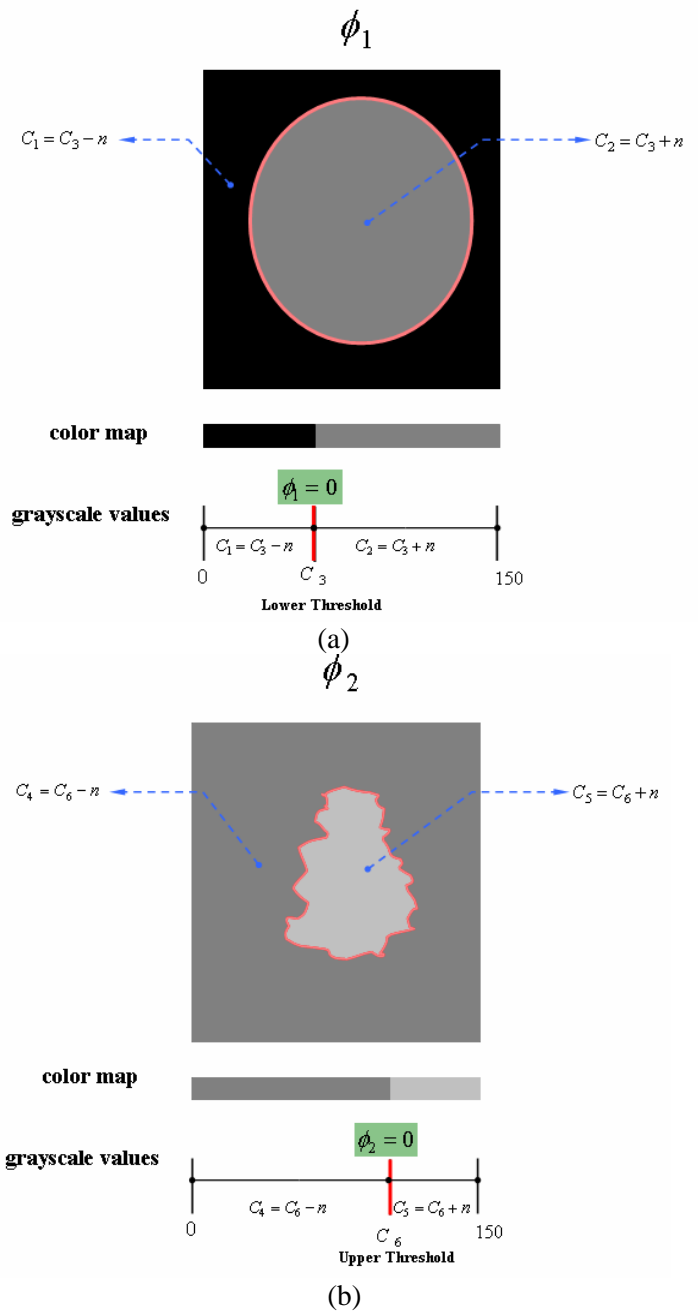


Fig. 8 Synthetic image and ROI (the gray region)

We set $c_6 > c_3$ in equation 10 and define $c_3 =$ Lower Threshold , $c_6 =$ Upper Threshold, Fig. 9(a) shows we use $\phi = \phi_1$ and c_3 to capture the outer contour of ROI. Fig. 9(b) shows we use $\phi = \phi_2$ and c_6 to capture the inner contour of ROI. Let $\phi = \phi_2 - \phi_1$, then the level sets of $\phi = 0$ are the outer and inner contours of ROI as shown in Fig. 9(c).



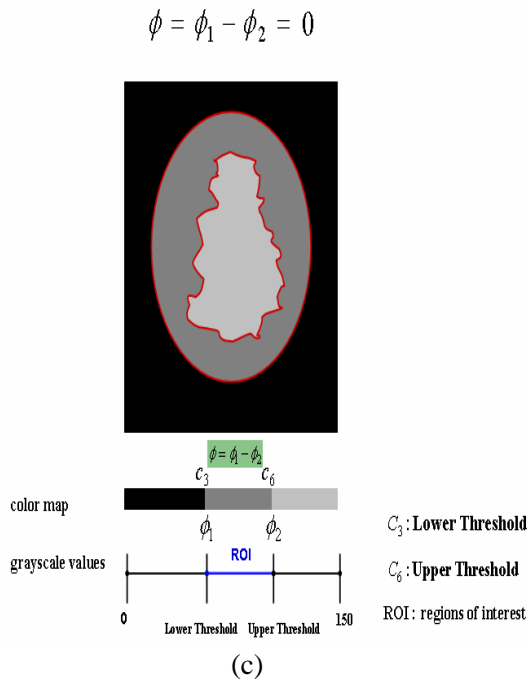


Fig. 9 (a) outer contour obtained with c_3 and ϕ_1 ; (b) inner contour obtained with c_6 in ϕ_2 and (c) both outer contour and inner contours obtained with $\phi = \phi_1 - \phi_2$

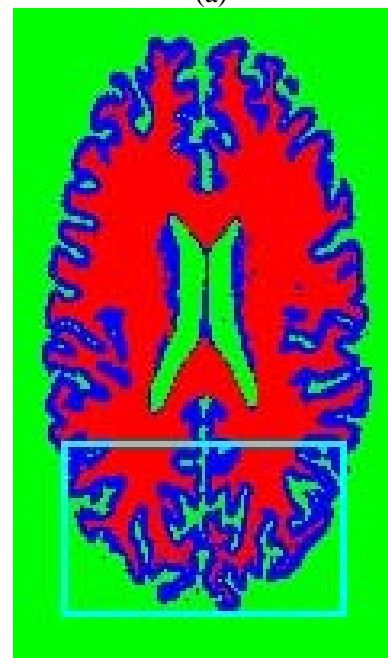
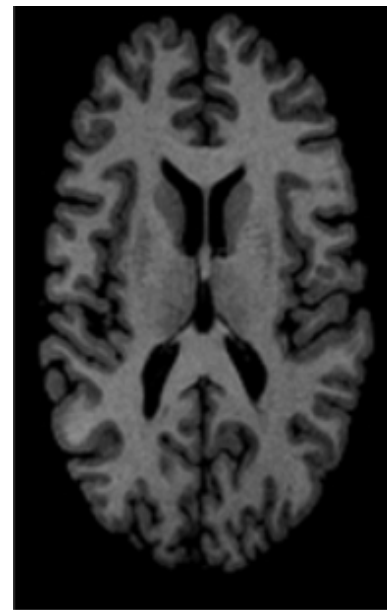
2.3. Automatic Selection of Threshold parameters

Automatic selection of threshold parameters is important for the accuracy and efficiency segmentation of brain image. The popular image segmentation method such as Fuzzy C-Means (FCM) algorithm [7][8] is not suitable for the segmentation of brain MR image. We will discuss the shortness of FCM algorithm in the section and proposed a modified algorithm for automatic selection of threshold parameters.

2.3.1 Fuzzy C-Means Algorithm

FCM algorithm is one kind of cluster analysis and used to solve unsupervised learning problems. FCM algorithm can be used to determine the Upper threshold (UT) and Lower threshold (LT). The task of FCM algorithm is a process of clustering data points to one of the groups. FCM has five steps in each iteration: 1. Set groups number 2. Initialize the fuzzy membership 3. Compute centroids and objective function 4. Update the fuzzy membership and 5. Convergence Test. We used FCM to classify all the pixels of the 67th slice brain image fig. 10(a)

into three and four groups as shown in fig. 10(b) and (c). The three groups are represented by red, green and blue colors and add yellow as a new group to construct four groups. To enlarge the difference between fig. 10(b) and (c), fig. 10(d) and (e) are respectively enlarged pictures of rectangle portion of the fig. 10(b) and 10(c). The pixels in red, green and blue colors represent tissues of WM, CSF or background and GM.



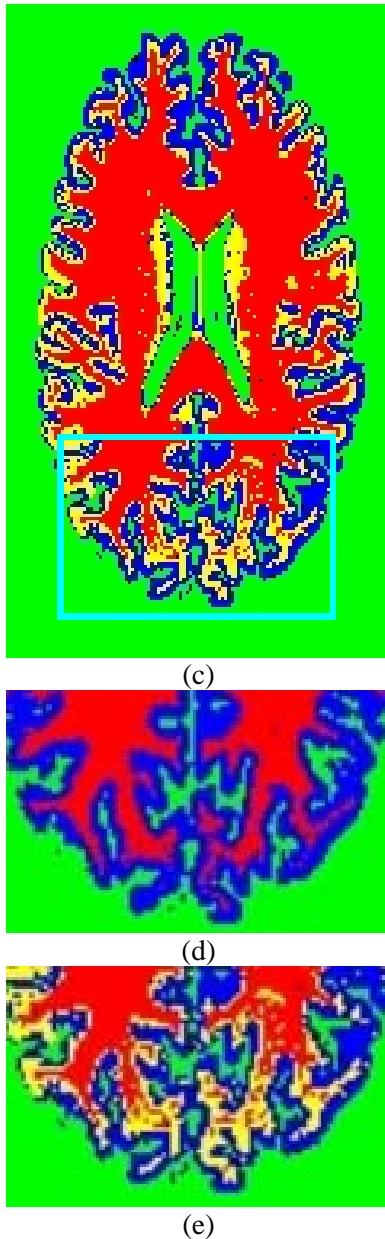


Fig. 10 Clustering results of brain image (a) by FCM with groups (b) 3 (d) 4 and (b)(c) are enlarged pictures of rectangle in (d) (e)

The intensity distributions of pixels in the three regions marked by three colors as shown in fig. 10(b) are listed in table1.

Table1 Three groups are classified by FCM as shown in Fig. 10(b).

Color	Green (CSF&Background)	Blue(GM)	Red (WM)
	(g, G)	(b, B)	(r, R)
Interval of intensity	(0,29)	(29,83)	(83,138)

The intensity distributions of pixels in the four regions marked by four colors as shown in fig. 10(c) are listed in Table2.

Table 2 Four groups are classified by FCM as shown in Fig. 10(c)

Color	Green (CSF&Background) (g, G)	Blue(GM)	Yellow (y, Y)	Red(WM)
Interval of intensity	(0,24)	(24,63)	(63,94)	(94,138)

As shown in table 2, the intensities of pixels in yellow region do not belong to GM or WM, but they belong to GM or WM, in three groups in table1. Some pixels in red and blue groups in table1 will be reassigned into the yellow group in table2 if the number of group increases from 3 to 4. We know the interval of GM is (29, 83) and the interval of WM is (83,138) in table 1; on other hand, the interval of GM is (24, 63) and the interval of WM is (94,138) in table 2. It is reasonable to guess the optimal lower limit of WM is between 63 and 94, but it may not be 83 and can not be obtain by FCM. As the reasons, FCM can not segment the MR brain image more accurately.

2.3.2 Fuzzy C-Means Algorithm

The WM, GM and CSF tissues can be segmented by ATLSWE Model. In order to obtain segmentations of WM, GM and CSF in brain images, we use the intervals obtained by FCM algorithm to find two parameters, LT and UT for ATLSWE Model described in section 2.2. Then the GM or WM tissue can be segmented by the active contours. The inner contours of GM are the outer contours of WM. We show the rules for selection of UT and LT for WM, GM and CSF tissues. Summary of the steps for selection of threshold parameters are listed as follows:

- (1) Set $c=3$, then obtain blue interval $[b, B]$ and red interval $[r, R]$
 - (2) Set $c=4$, then obtain yellow interval $[y, Y]$
 - (3) Compute Lower Threshold LT and Upper Threshold UT
- Selection UT and LT for WM:

In table 1 the intervals of GM is (b, B) and the interval of WM is (r, R). The yellow interval is (y, Y) in table 2. We find a good rule for choice of UT is B and LT is as follows:

If $B > y$

$$LT = (B+y)/2$$

else

$$LT = B$$

End if

The rule can be transformed to a decision function by LT Heaviside function or unit step function $H(x)$ which is defined by:

$$H(x) = \begin{cases} 1, & x > 0 \\ 0 & x \leq 0 \end{cases} \quad (10)$$

and

$$LT = \left\lceil \frac{(B+y) \times H(B-y) + 2B \times [1 - H(B-y)]}{2} \right\rceil \quad (11)$$

Selection UT and LT for GM:

In table 1 the intervals of GM is (b, B) and the interval of WM is (r, R). The yellow interval is (y, Y) in table 2. We find a good rule for choice of UT is B and LT is as follows:

If $b < G$

$$LT = (G+b)/2$$

else

$$LT = G$$

End if

The rule can be transformed to a decision function LT by Heaviside function $H(x)$.

$$LT = \left\lceil \frac{2G \times H(b-G) + (b+G)[1 - H(b-G)]}{2} \right\rceil \quad (12)$$

The boundary between CSF and GM is used to select the UT of CSF equaling to the LT of GM and LT of CSF is chosen zero (g) as shown in table 2.

2.4. Similarity index

The segmentations of GM were compared with the gold standard (by mrGray) by counting the number of pixels. The segmentation with the gold standard was indicated by the similarity index (SI) [23]. This is a measure of the correctly classified tissue area. The similarity index SI is defined as:

$$SI = \frac{2 \times Inter}{GS + Object} \quad (13)$$

Where GS denotes the gold standard of the WM segmentation, and Object is the segmentation result by 『Adaptive Threshold Level Set Without Edge Model』. Inter denotes the intersection of the gold standard and Object. The definition is shown in Fig. 11.

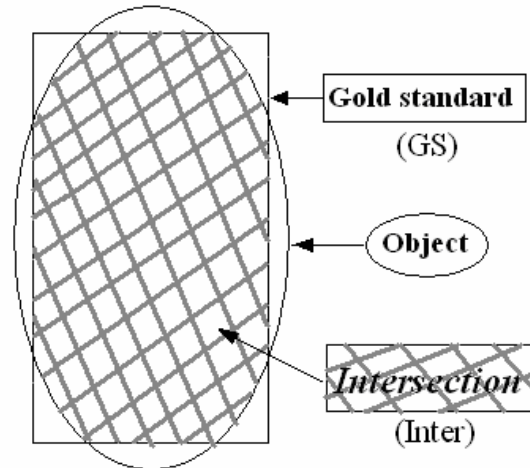
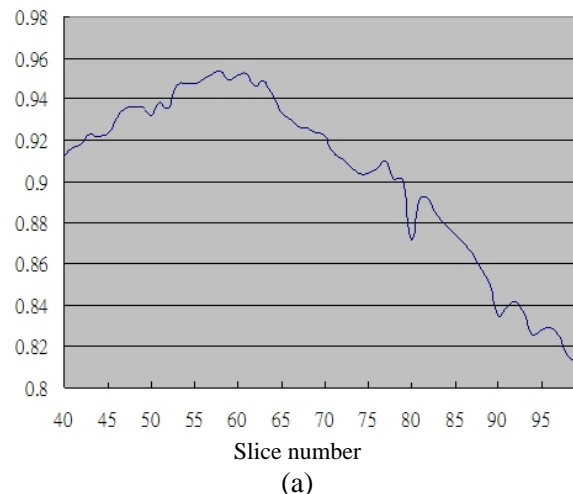
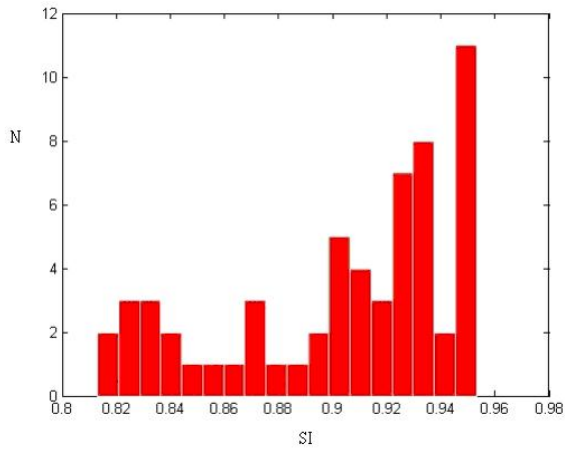


Fig. 11 The definition of similarity index (SI)

3. RESULTS AND DISCUSSION

We show the segmentation results of sixty images with number between 40th and 99th by 『ATLSWE Model』 to evaluate its accuracy. Comparing the segmentation results with the golden standard results, the SI values are calculated as defined in the equation (13) and shown in Fig. 12(a) with the maximum 0.95307 and minimum 0.8131. A histogram of SI is shown in the Fig. 12(b) with the mean value 0.90311 and the variance 0.042049. The parameter “N” in the Fig. 12(b) is the times of SI values appeared.

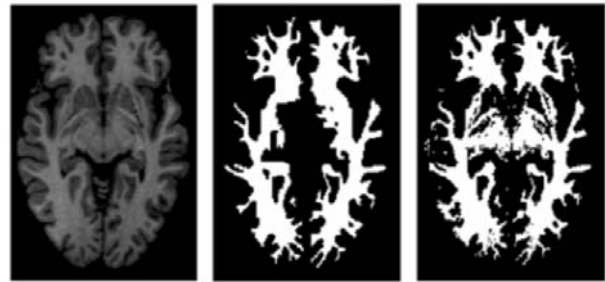




(b)

Fig. 12 (a) The similarity indices curve and (b) histogram obtained from 40th to 99th MR images.

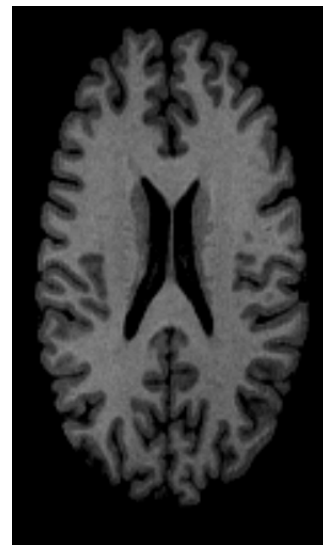
The first test image as shown in the Fig. 13(a) with the number 60 and SI 0.9515 in Fig. 12(a). The other image as shown in the Fig. 13(b) with the number 94 and SI 0.8252 in Fig. 12(a). Comparing the original images in Fig. 13(a) and Fig. 13(b), the anatomy atlas is different. As shown in center of Fig. 13(b), the sup colliculus is not appear in the golden standard, but it appears in the segmented object as shown in the right of Fig. 13(b). Comparing the golden standard and the segmented object, they are vary similar in Fig. 13(a), but not similar in Fig. 13(b). Although the SI value of 94th image is smaller than the mean value of SI, but the outer contours of the white mater in Fig. 13(a) and Fig. 13(b) are almost the same. For the purpose of three dimensional surface reconstruction of WM, the segmentation result is very useful.



(b) original image (left), gold standard (center) and segmented object (right)

Fig. 13 The 60th slice (a) and the 94th slice (b) with the golden standard and segmented object.

Fig. 14(a) is the original brain MR image. Chan-Vese model can not meet our desire contour as shown in Fig. 14(b) because the c_1 and c_2 are not constants decided by us. Fig.11(c), (d) and (e) show the WM, GM and CSF segmented results by ATLSWE Model with threshold parameters with (c) LT=83,UT=140, (d) LT=27,UT=83 (e) LT=0, UT=27.



(a)



(a) original image (left), gold standard (center) and segmented object (right)

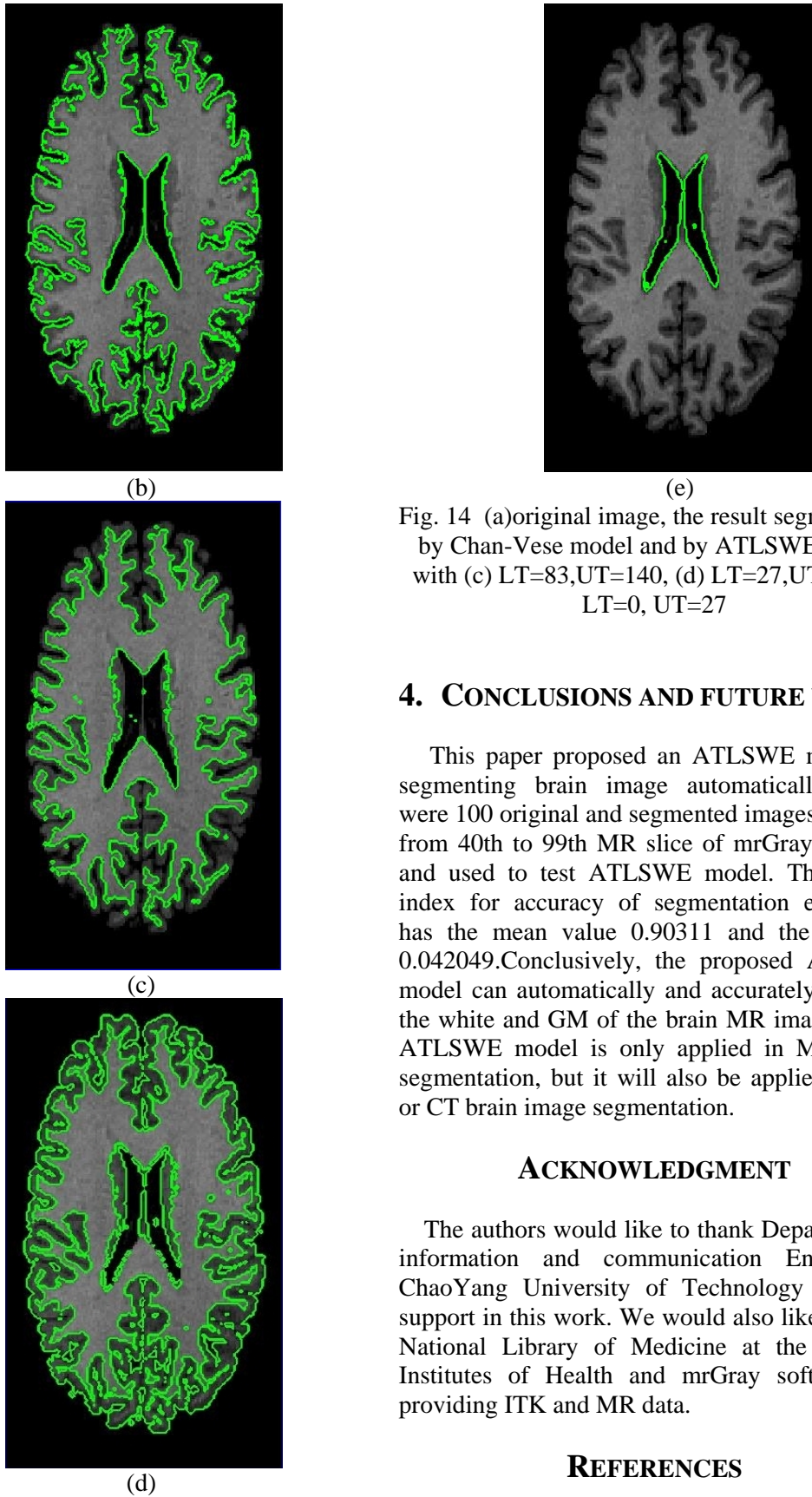


Fig. 14 (a)original image, the result segmented (b) by Chan-Vese model and by ATLSWE Model with (c) $LT=83, UT=140$, (d) $LT=27, UT=83$ (e) $LT=0, UT=27$

4. CONCLUSIONS AND FUTURE WORK

This paper proposed an ATLSWE model for segmenting brain image automatically. There were 100 original and segmented images obtained from 40th to 99th MR slice of mrGray software and used to test ATLSWE model. The similar index for accuracy of segmentation evaluation has the mean value 0.90311 and the variance 0.042049. Conclusively, the proposed ATLSWE model can automatically and accurately segment the white and GM of the brain MR images. Now ATLSWE model is only applied in MR image segmentation, but it will also be applied in PET or CT brain image segmentation.

ACKNOWLEDGMENT

The authors would like to thank Department of information and communication Engineering ChaoYang University of Technology for their support in this work. We would also like to thank National Library of Medicine at the National Institutes of Health and mrGray software for providing ITK and MR data.

REFERENCES

- [1] Dhawan, A.P., Medical Image Analysis, 2003. John Wiley Publications and IEEE Press, pp175.

- [2] Morrison, M., Attikiouzel, Y., 1992. "A probabilistic neural network based image segmentation network for magnetic resonance images". In Proc. Conf. Neural Networks. Vol. 3. pp. 60–65.
- [3] Ozkan, M., Dawant, B., Maciunas, R., 1993. "Neural-network-based segmentation of multimodal medical images: a comparative and prospective study". IEEE Trans. Med. Imaging, 12, 534–544.
- [4] Kollokian, V., 1996. Performance analysis of automatic techniques for tissue classification in MRI of the human brain. Master's thesis, Concordia University, Montreal, Canada.
- [5] Wang, Y., Adah, T., Kung, S.-Y., 1998. Quantification and segmentation of brain tissues from MR images: A probabilistic neural network approach. IEEE Transactions on Image Processing 7 (8), 1165–1181.
- [6] Bezdek, J.C., Hall, L.O. and Clarke, L.P.: Review of MR Image Segmentation Techniques Using Pattern Recognition. 20, (1993) 1033–1048.
- [7] Bezdek, J.C. , 1981. "Pattern Recognition with Fuzzy Objective Function Algorithms". Plenum Press, New York.
- [8] Dunn, J.C., 1974. "A Fuzzy Relative of the ISODATA Process and Its Use in Detecting Compact Well-Separated Clusters". Journal of Cybernetics., 3, pp 32-57.
- [9] Kass, M., Witkin, A., and Terzopoulos, D. , 1987. "Snakes - Active Contour Models". International Journal of Computer Vision, 1(4):321-331.
- [10] Osher S. and Sethian J.A., 1988. "Fronts propagating with curvature dependent speed: Algorithms based on Hamilton-Jacobi formulations." Journal of Computational Physics, 79:12-49.
- [11] Sethian, J. A., 1999. Level set methods and fast marching methods: evolving interfaces in computational geometry, fluid mechanics, computer vision and materials science. Cambridge University Press, Cambridge, UK.
- [12] Hoffmann, T. J., Chung, M. K., Dalton, K. M., Alexander, A. L., Wahba, G., Davidson, R. J., 2004. Subpixel curvature estimation of the corpus callosum via splines and its application to autism. 10th Annual Meeting of the Organization for Human Brain Mapping. <http://www.stat.wisc.edu/~mchung/papers/HBM2004/HBM2004thomas.html>.
- [13] Tohka, J., Zijdenbos, A., Evans, A. C., 2004. Fast and robust parameter estimation for statistical partial volume models in brain MRI. NeuroImage 23 (1), 84–97.
- [14] Mumford, D., Shah, J., 1985. Boundary detection by minimizing functionals. In IEEE Computer Society Conference on Computer Vision and Pattern Recognition (CVPR). pp. 22–26.
- [15] Malladi, R., Sethian, J.A., Vemuri, B.C., 1995. "Shape modeling with front propagation: A level set approach". IEEE Trans. on Pattern Analysis and Machine Intelligence 17 158-175.
- [16] Lefohn, A., Kniss, E., Hansen, J., C., and Whitaker, R., 2003. "Interactive deformation and visualization of level set surfaces using graphics hardware". In IEEE Visualization, pp. 497-504.
- [17] Zchang, Z.U., and Hsu, C.Y., 2005. "Automatic Segmentation by Threshold Level Set Method with Adaptive Parameters" CVGIP conference in Taiwan.
- [18] N. Otsu, 1979. "A threshold selection method from gray-level histograms,". IEEE Transactions on Systems, Man, and Cybernetics, vol. 9, no. 1, pp. 62-66.
- [19] Chan, T.F., Vese, L.A., 2001. Active Contours Without Edges. IEEE Trans. on Image Processing. 10(2), 266-277.
- [20] Teo, P.C., Sapiro, G. and Wandell, B.A., 1997. "Creating connected representations of cortical grey matter for functional MRI visualization". IEEE Transactions on Medical Imaging, 16: 852-863.
- [21] Wandell, B., Chial S., and Backus, B., 2000. "Visualization and Measurement of the Cortical Surface". Journal of Cognitive Neuroscience, vol. 12, no. 5. pp. 739-52.
- [22] Kapur, T., W. Eric L. Grimson, William M. Wells III, Kikinis. R., 1996. "Segmentation of brain tissue from magnetic resonance image". Medical Image Analysis volume 1, number 2, pp 109-127.
- [23] Zijdenbos, A.P., Dawant, B.M., Margolin, R.A., and Palmer, A.C. , 1994. "Morphometric analysis of white matter lesions in MR images: method a validation. " IEEE Trans. Med. Imaging 13, 716-724.

APPENDIX

Calculus of variations is a field of mathematics that deals with functionals. The

extremal function makes the functional attain a maximum or minimum value. For example, the functional $E(c_1, c_2, \phi)$ can be formed as integrals by the equation (A1).

$$E(c_1, c_2, \phi) = \mu \int_{\Omega} |\nabla H(\phi)| dx dy + \int_{\Omega} (u_0 - c_1)^2 H(\phi) dx dy + \int_{\Omega} (u_0 - c_2)^2 (1 - H(\phi)) dx dy \quad (A1)$$

Solution of the variational problem may be obtained by solving the associated Euler-Lagrange equation. In order to illustrate this process of finding Euler-Lagrange equation, we consider a function ϕ equals to ϕ^* plus a variation $t\psi$ and it is $\phi = \phi^* + t\psi$. Where the function ψ is an arbitrary function with a boundary condition $\psi|_{\partial\Omega} = 0$ and the function ϕ^* is an extremal function when the independent variable t is zero. We use the necessary condition $\delta E|_{\phi=\phi^*} = 0$ to find extremal function ϕ^* .

The necessary condition $\delta E|_{\phi=\phi^*} = 0$ is equivalent to the following condition that is formed as derivatives with respect to independent variable t .

$$\frac{dE}{dt} \Big|_{t=0} = 0 \quad (A2)$$

In the equation (A1), we use (A3) to denote the term $\mu \int_{\Omega} |\nabla H(\phi)| dx dy$ as following:

$$\mu \int_{\Omega} |\nabla H(\phi)| dx dy \quad (A3)$$

Then (A3) can be denoted by $\mu \ell(\phi)$ and $\ell(\phi)$ can be derived and changed as follow:

$$\ell(\phi) = \int_{\Omega} |\nabla H(\phi)| dx dy = \int_{\Omega} \delta_{\varepsilon} |\nabla \phi| dx dy \quad (A4)$$

The second and third terms are denoted by $E_1 = \int_{\Omega} (u_0 - c_1)^2 H(\phi) dx dy$ and

$$E_2 = \int_{\Omega} (u_0 - c_2)^2 (1 - H(\phi)) dx dy.$$

The left side of equation (A2) can be formulated as the equation (A5).

$$\frac{dE}{dt} \Big|_{t=0} = \mu \frac{d\ell(\phi^*)}{dt} + \frac{dE_1}{dt} + \frac{dE_2}{dt} \quad (A5)$$

The first term $\mu \frac{d\ell(\phi^*)}{dt}$ in equation (A5) can be derived as shown by equation (A6).

$$\mu \frac{d\ell(\phi^*)}{dt} = - \iint_{\Omega} \mu \delta_{\varepsilon}(\phi^*) \nabla \cdot \frac{\nabla \phi}{|\nabla \phi|} \psi dx dy \quad (A6)$$

The second term $\frac{dE_1}{dt}$ in equation (A5) can be derived and obtained as equation (A7).

$$\frac{dE_1}{dt} \Big|_{t=0} = \frac{\partial E_1}{\partial c_1} \frac{\partial c_1}{\partial \phi} \frac{d\phi}{dt} + \frac{\partial E_1}{\partial \phi} \frac{d\phi}{dt} \quad (A7)$$

Different from the condition of Chan-Vese model $\frac{\partial E_1}{\partial c_1} = 0$, we assume c_1 is constant

($\frac{\partial c_1}{\partial \phi} = 0$) and substitutes it into equation (A7).

$$\frac{dE_1}{dt} \Big|_{t=0} = \frac{\partial E_1}{\partial \phi} \frac{d\phi}{dt} = \int_{\Omega} (u_0 - c_1)^2 \delta(\phi^*) \psi dx dy \quad (A8)$$

The third term $\frac{dE_2}{dt}$ in equation (A5) can be derived and obtained as equation (A9).

$$\frac{dE_2}{dt} \Big|_{t=0} = \frac{\partial E_2}{\partial c_2} \frac{\partial c_2}{\partial \phi} \frac{d\phi}{dt} + \frac{\partial E_2}{\partial \phi} \frac{d\phi}{dt} \quad (A9)$$

Different from the condition of Chan-Vese model $\frac{\partial E_2}{\partial c_2} = 0$, we assume c_2 is constant

($\frac{\partial c_2}{\partial \phi} = 0$) and substitutes it into equation (A9).

$$\frac{dE_2}{dt} \Big|_{t=0} = \frac{\partial E_2}{\partial \phi} \frac{d\phi}{dt} \quad (A10)$$

$$= - \int_{\Omega} (u_0 - c_2)^2 \delta(\phi^*) \psi dx dy$$

Substituting equations (A6), (A8) and (A10) into equation (A2), we have the equation (A11).

$$\iint_{\Omega} \delta_{\varepsilon}(\phi^*) \left[-\mu \nabla \cdot \frac{\nabla \phi^*}{|\nabla \phi^*|} + (u_0 - c_1)^2 - (u_0 - c_2)^2 \right] \psi dx dy = 0 \quad (A11)$$

Because the function ψ is an arbitrary function in the equation (A11), then one obtains

$$\delta(\phi^*) \left[-\mu \nabla \cdot \frac{\nabla \phi^*}{|\nabla \phi^*|} + (u_0 - c_1)^2 - (u_0 - c_2)^2 \right] = 0 \quad (A12)$$

To solve the optimal function ϕ^* of equation (A12) iteratively, the following equation (A13) is adopted.

$$\frac{\partial \phi}{\partial t} = \delta_{\varepsilon}(\phi) \left(\mu \nabla \cdot \frac{\nabla \phi}{|\nabla \phi|} - (u_0 - c_1)^2 + (u_0 - c_2)^2 \right) \quad (A13)$$